Topological Characterization of Porous Media

Hans-Jörg Vogel

University of Heidelberg, Institute of Environmental Physics,
INF 229, 69120 Heidelberg, Germany

Abstract. It is an attractive approach to predict flow and in based on direct investigations of their structure. The most crucial property is the of the structure because it is difficult to measure. This is true both at the pore scale, which may be represented as a binary structure, and at a larger scale defined by continuous macroscopic state variables as phase density or . At the pore scale a function is introduced which is defined by the as a function of the pore diameter. This function is used to generate of the porous structure that allow to predict bulk hydraulic properties of the material. At the continuum scale the structure is represented on a grey scale representing the porosity of the material with a given resolution. Here, topology is quantified by a connectivity function defined by the Euler characteristic as a function of a porosity threshold. Results are presented for the structure of natural soils measured by . The significance of topology at the continuum scale is demonstrated through numerical simulations. It is found that the effective permeabilities of two heterogeneous having the same auto-covariance but different topology differ considerably.

1 Introduction

Flow and transport within porous media are governed by their porous structure. This is true at a small scale of single pores but also at a larger scale where the structure of continuous fields of hydraulic properties such as the hydraulic permeability becomes relevant. It is an old scientific challenge to predict the behavior of porous media from some structural properties which are directly observable so that no expensive experiments are required.

Nowadays, more and more techniques are available to directly investigate the structure of porous media. Especially X-ray tomography has become an attractive technique capable to detect pore structure with high resolution of some 0.01mm [21] which is also presented by Arns et al. [2] in this volume. At a larger scale the structure of density or porosity at resolutions of some 1.0 mm can be measured by X-ray tomography [39]. Nanotomography as a 3D-image tool by scanning microscopy is presented in this volume by Magerle [22]. In this paper, soil as one of the most complex porous media is considered.

To bridge the gap between structure and function the quantification of relevant structural properties is required. At the pore scale, the size distribution of pores is important while at the larger continuum scale the pore-scale effects may be smeared out and the autocorrelation of permeabilities may play a crucial role. Besides these metric properties, also the topology of the structure is highly relevant for any kind of transport, meaning the way the structural units are interconnected in space. This was demonstrated at the pore-scale [20, 43] and at the continuum scale for the permeability field of an aquifer [45].

K.R. Mecke, D. Stoyan (Eds.): LNP 600, pp. 75–92, 2002.

Moreover, the shape of structural units may be quantified using Minkowski functionals, see [2, 3] in this volume. An overview on quantitative methods for the characterization of porous media can be found in the precurser to this volume [26].

The focus of this contribution is on topology where quantitative information is still hard to get. This is because a topological description of a three dimensional structure requires information at a resolution corresponding to the size of the structural units, e.g. pores, in all three dimensions. There are no stereological methods to infer 3D topological characteristics from two dimensional sections. Hence, measurements of connectivity typically requires a complete three dimensional analysis of the structure or at least a representative elementary volume (REV). This can be achieved for simple isotropic media as sandstones where a few cubic millimeters may be sufficient to fully characterize the porous structure. Here, local percolation probabilities [15] can successfully applied to characterize topology. In more heterogeneous porous media where the structural units are extremely anisotropic, e.g. root channels, cracks and earthworm borrows in , a representative three dimensional sample is extremely expensive and most topological measures are afflicted with unacceptable uncertainties at the edges.

In this paper connectivity functions for the pore scale and for continuous fields are introduced which are based on the Euler characteristic. An important advantage of this approach is the fact that an unbiased estimation of the Euler characteristic is possible from local measurements, meaning there are no edge effects and the shape of the required three dimensional sample is irrelevant.

The paper is organized as follows. In the first section the connectivity function for binary pore structures is defined as the Euler characteristic as a function of the pore size. In the second part it is demonstrated how to adapt a pore network model to a given and connectivity function. Numerical simulations of effective hydraulic properties based on network models are compared to direct experimental findings to demonstrate the effect of topology. In the third section the same concept is applied to continuum fields, where the connectivity function is defined as the Euler characteristic in dependency of the threshold applied to the continuous field. This approach is demonstrated for the structure of porosity in a Loess soil measured by X-ray tomography. Finally, the significance of topology is demonstrated for water flow in random permeability fields having the same but different topology.

2 Pore Scale Topology

Besides the porosity and the size distribution of pores, the topology of the pore space is a crucial property regarding flow and transport in porous media. The way how pores are interconnected may be even more important than their number and size.

The basic topological properties are the number N of isolated objects, i.e. pores, and the number of redundant connections C within the pores space, and, in three dimensions, the number of completely enclosed cavities H [14]. For a detailed discussion of these measures see the contribution of Robins [34] in this volume. The Euler characteristic χ combines the basic topological measures to

$$\chi = N - C + H \; . \tag{1}$$

Hence, the Euler characteristic is a measure of connectivity which gives positive values for poorly connected structures where $N > C$ and negative values for more connected structures where $N < C$. For the topology of a network of pores in natural porous media, the quantity H is of minor importance since solid particles completely surrounded by pores are rare. An essential advantage for the measurement of χ is the fact that an unbiased estimation of χ is possible for a 3D cutout of the porous media. Thereby, the basic quantities N, C and H are not counted explicitely but the Euler characteristic may be deduced from the local geometry of the structure [38, 8]. This is demonstrated for the application to digitized images in the contribution of Ohser et al. [27] in this volume.

The corresponding algorithms for binary digitized images are straightforward [28, 40]. Consequently, we may obtain χ from two parallel serial sections as a minimum three dimensional sample also referred to as disector [38, 8].

This is of practical importance in such media where a full three dimensional representation is hard to get and this is rather the rule than the exception. The complete structure or a representative elementary volume in terms of topology is typically not available. In most cases we are restricted to some small subsamples for which the possible determination of N, C and H would be unacceptable due to the uncertainty at the edges of the investigated cutout. To estimate the Euler characteristic, however, a small stack of serial sections may be sufficient. This was demonstrated for the pore structure of a soil [41]. Thereby, the number of serial sections can be reduced to the benefit of the size of the individual sections in order to sample the structure more representatively and thus, to arrive at a more reliable estimation of χ [44]. This aspect is illustrated in Fig. 1.

Another approach towards the quantification of topology in porous media is the measure of percolation probabilities denoting the probability to find a continuous path through a sample of a given size. Percolation probabilities can be evaluated as a function of sample size and porosity. This leads to connectivity functions [16, 17] which may be related to effective properties of the material [46]. However, a prerequisite of this approach is the knowledge of the complete structure or at least a representative subsample. Hence, the same problems as for the determination of N, C and H are encountered. For isotropic structures as e.g. sandstone, however, percolation probabilities provide the topological information required [18].

In the following, a connectivity function is introduced which is based on the Euler characteristic χ and can thus be determined from local measurements using a small stack of serial sections. Figure 1 shows an example of the heterogeneous structure of pores in a silty clay soil. For a detailed description of this material and the sampling technique see [41].

Topological characteristics of porous media depend on the spatial resolution of the available data. This is true if pores exist which are in the size range of the resolution or smaller. Then, the connectivity of the porous structure is expected to change with resolution because more connections or more isolated features appear.

The idea of the connectivity function proposed here is to measure the Euler characteristic as a function of pore size. Starting with the largest pores, which may be isolated and not connected, the smaller pores are successively added which change the topology in a characteristic way, e.g. in soil we expect an increase of connectivity. This kind of connectivity function yields an integral description of the overall topology and should

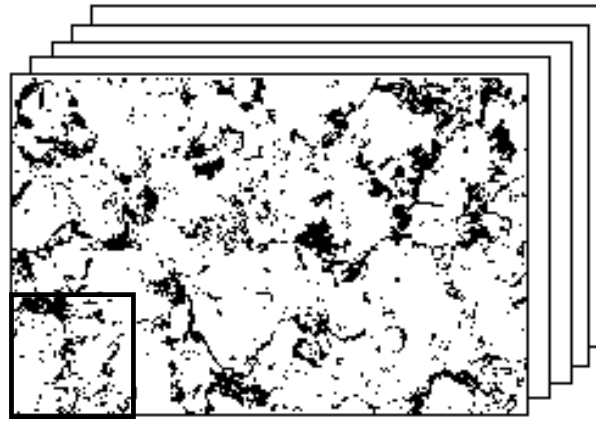

Fig. 1. One of 20 serial sections through undisturbed silty clay soil used to determine the Euler characteristic. Natural width is 20 mm, resolution is 0.013 mm/pixel, separation of serial sections is 0.4 mm, pores are black. The square in the lower left corner represents the size of a cube having the same volume as a pair of serial sections.

reflect the hydraulic behavior of the material because it contains information on the way how pores of different size are interconnected.

As a prerequisite, a criteria of pore size is required. Morphological granulometry [37] provides an excellent tool to filter pores which are smaller than a given threshold. It is based on morphological erosions and dilations using a spherical structuring element. Based on a binary three dimensional sample $\mathbb{S}$ including the subset of pores $\mathbb{P} \subset \mathbb{S}$, the eroded set $\mathbb{P}_{\mathrm{erod}}$ is obtained as

$$\mathbb{P}_{\mathrm{erod}} = \{x : \mathbb{B}_x^d \subset \mathbb{P}\} \; = \; \mathbb{P} \ominus \mathbb{B}^d \tag{2}$$

where $\mathbb{B}_x^d$ is the sphere with diameter d centered at point x. Consequently $\mathbb{P}_{\mathrm{erod}}$ describes the set of all locations within $\mathbb{P}$ where the structuring element fits completely into the pore space. The morphological dilation is defined as

$$\mathbb{P}_{\mathrm{dil}} = \{x : \mathbb{B}_x^d \cap \mathbb{P} \neq \emptyset\} \; = \; \mathbb{P} \oplus \mathbb{B}^d \tag{3}$$

The morphological opening combines and :

$$\mathbb{P}_{\mathrm{op}} = (\mathbb{P} \ominus \mathbb{B}^d) \oplus \mathbb{B}^d \tag{4}$$

which removes all pores smaller than the structuring element $\mathbb{B}^d$. Starting with a three dimensional image recorded at a given resolution λ, the application of n structuring elements $\mathbb{B}^d$ with increasing diameter $d = n\lambda$ produces realizations $\mathbb{P}_{\mathrm{op}}(d)$ of the porous structure where only pores $> d$ are considered. Hence, a cumulative pore size distribution can be defined as

$$F(d) = \Phi(\mathbb{P}_{\mathrm{op}}(d)) \tag{5}$$

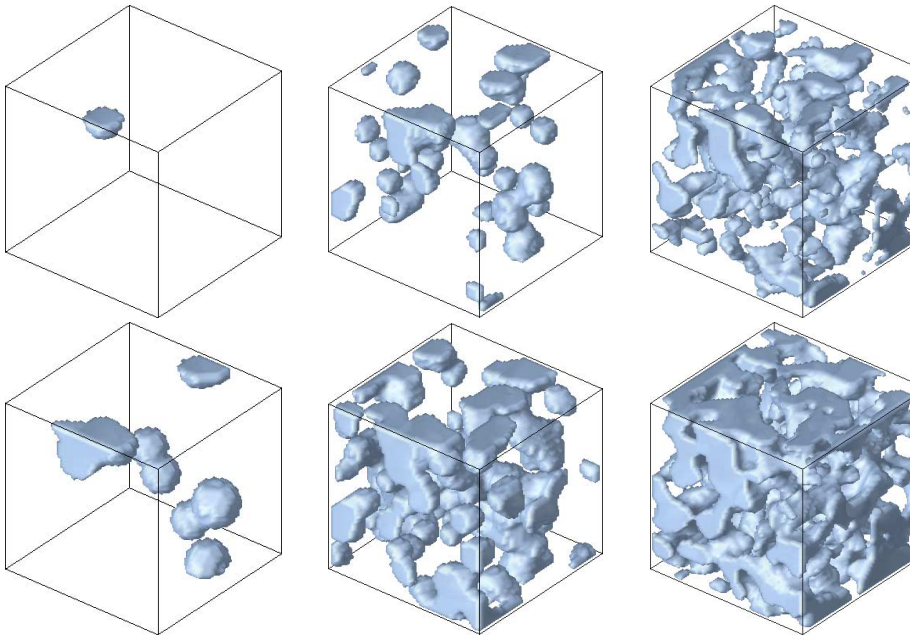

Fig. 2. Simulated pore structures from excursion sets according to different thresholds $t = 100$ upper row and $t = 120$ lower row. From left to right: isosurfaces for pores $\mathbb{P}_{\mathrm{op}}(d)$ with decreasing minimum diameter d. The related connectivity functions are shown in Fig. 3.

where $\Phi()$ means 'porosity of'. The size criteria used here reflects almost perfectly our idea of the 'hydraulic diameter' of a pore. Now, the Euler characteristic χ can be determined as a function of d by calculating χ for the different $\mathbb{P}_{\mathrm{op}}(d)$ to obtain the connectivity function $\chi(d)$. It should be noted that for the calculation of $\chi(d)$ a three dimensional sample is required where all dimension exceed the maximum pore diameter so that $\mathbb{P}_{\mathrm{op}}(d)$ can be determined. Hence, a number of serial sections is required and a disector is not sufficient. Moreover it should be noted that the opened set $\mathbb{P}_{\mathrm{op}}(d)$ may include short necks that are smaller than the diameter of the structuring element. This could be avoided by using $\mathbb{P}_{\mathrm{erod}}(d)$.

To demonstrate the behavior of $\chi(d)$ for a simple isotropic structure, a three dimensional porous media was modeled as an excursion set of a Gaussian random field [30, 32]. The random field was generated according to a predefined auto-covariance function. It was then segmented into pores and solid according to a given threshold t meaning all values $< t$ are considered to be pores. In Fig. 2 (right) the obtained porous structure is illustrated as an isosurface according to two different thresholds t. Clearly, the structure is more intensely connected for higher values of t.

The corresponding connectivity functions are shown in Fig. 3. Generally, the connectivity increases with decreasing pore size d and with increasing porosity. The latter is controlled by the threshold t of the Gaussian random field. For high porosities ($t = 150$) connectivity decreases for small d because there are completely enclosed cavities H

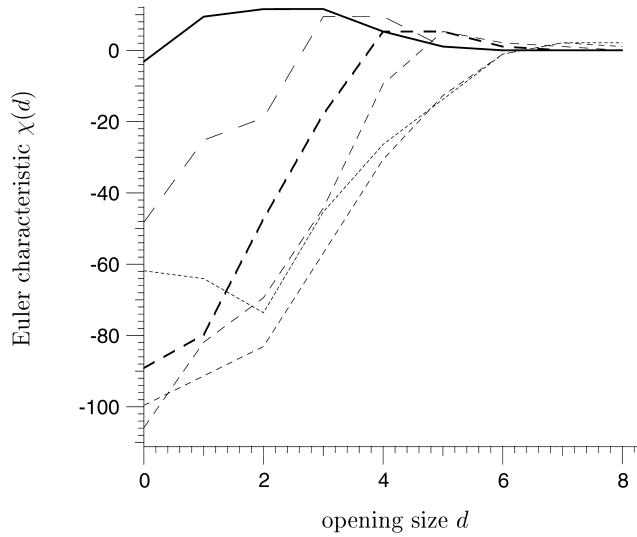

Fig. 3. Connectivity functions of excursion sets related to different threshold values $t \in 100, 110, 120, 130, 140, 150$ (decreasing dash length) applied to the Gaussian random field . Thick lines are the results for t = 100 and t = 120 which are illustrated in Fig. 2.

within the pore space, see (1). In natural porous media, however, this behavior is not expected, since solid clusters completely surrounded by pores are rare.

3 Pore Network Modeling

Network models are idealized representations of the complex pore geometry which may be used to calculate effective hydraulic properties of porous media. This approach was introduced by [9, 10, 11] and subsequently developed in the field of petroleum engineering [7, 6] but also in the field of soil physics and hydrology [4, 5].

The calculation of effective permeabilities or the pressure-saturation relation of network models is straightforward. Hence network modeling is an efficient tool to investigate the effect of geometrical aspects on the effective behavior of porous media [20, 12, 13]. If network models are intended to provide predictions of hydraulic properties [47, 31], the geometry of the network has to be adopted to some relevant observables of the porous structure. Thereby, topology is typically not considered explicitely, because direct measurements are notorious difficult.

However, the connectivity function $\chi(d)$ defined in the previous section is a quantitative handle on topology. Using $\chi(d)$ together with the pore size distribution $F(d)$ as obtained from morphological openings, a network model may be generated which mimics the measured structure in terms of pore size and topology. The first question is, how to generate a network model that fulfills a predefined $\chi(d)$ and $F(d)$? And the second crucial question is, to what extend does such a network model reproduce the hydraulic behavior of the material which may be answered by comparing network simulations

with direct experiments. This work was presented in detail by [42, 44] and is reviewed here only briefly.

The basic geometry of the network is a face-centered cubic grid with grid constant λ and a coordination number $Z = 12$. The bonds represent cylindrical pores with radius r while the nodes have no extra volume. To reach a given Euler characteristic and porosity only a part of all available bonds $Z_{\text{eff}} < Z$ is used while the residual bonds $Z - Z_{\text{eff}}$ are interpreted to represent 'background porosity', i.e. small pores with diameter below the resolution of the available data. As demonstrated in [42] the unknown parameters λ and Z_{eff} can be directly calculated from the input functions $\chi(d)$ and $F(d)$. Then, the probability distribution of different classes of pore radii within the network can be directly obtained from $F(d)$.

The realization of $\chi(d)$, however, is more demanding. The Euler characteristic of a network model is simply obtained by

$$\chi = N_n - N_b \tag{6}$$

where N_n is the number of nodes to which at least one bond is connected, and N_b the total number of bonds; see also [23]. In order to realize a predefined connectivity function $\chi(d)$, we start with the generation of the largest pores. During the generation process the actual Euler characteristic χ_{act} of the network is continously updated using (6). Prior to attributing a radius d to a bond the difference between $\chi(d)$ and $\chi_{\text{act}}(d)$ is evaluated. If it is negative only an isolated bond can be chosen, otherwise only bonds connected to already existing pores are considered. In this way, a predefined connectivity function is realized. In Fig. 4, an example of such a network model including 8^3 nodes is shown. To simulate hydraulic properties 64^3 nodes were used.

Once the network geometry is generated effective hydraulic properties can be simulated. First, the pressure-saturation relation $\theta(\psi)$ is computed describing the water saturation θ in dependency of the capillary pressure ψ and second, the relative hydraulic conductivity function $K_r(\psi)$ describing the hydraulic conductivity relative to the conductivity at water saturation as a function of the capillary pressure ψ. To determine the fluid saturation for a given capillary pressure ψ each bond above a critical radius r_c is drained, provided that it is in contact with the non-wetting phase:

$$r_c > 2\sigma\psi^{-1} \tag{7}$$

This is in accordance with the Young-Laplace equation where σ is the surface tension and complete wetting is assumed, i.e. the contact angle between water and solid is zero. In Fig. 4 the distribution of the wetting and non-wetting phase at a certain capillary pressure is illustrated.

To calculate the hydraulic conductivity at different water saturations we assume Poiseuille flow within the cylindrical bonds of the network. Given a pressure gradient across the ends of the network, this leads to a system of linear equations which was solved by a conjugate gradient method [29].

In Fig. 5 simulation results are compared to experimental findings in a silty clay soil, for details see [42]. Considering the fact that the simulated results are only based on directly measured morphological data, i.e. $\chi(d)$ and $F(d)$, the agreement of the shape of $\theta(\psi)$ and $K_r(\psi)$ was found to be reasonably good. This means that the hydraulic

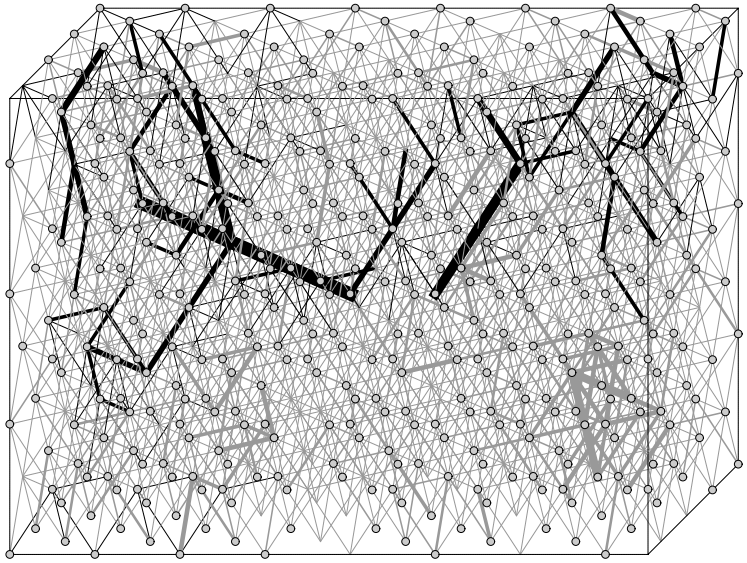

Fig. 4. Example of a networkmodel of 8^3 nodes at a certain capillary pressure where some pores are filled with water (grey) and others with air (black).

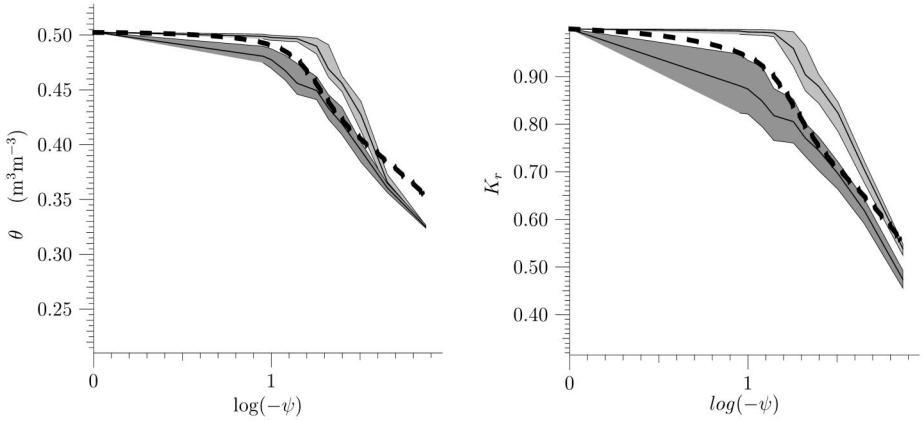

Fig. 5. Water characteristic $\theta(\psi)$ (left) and hydraulic conductivity function $K(\psi)$ (right) obtained from network models with random topology (light grey) and measured topology of a Loess soil (dark grey). The shaded areas enclose the maximum and minimum values of 20 realizations. The dashed line represents the experimental results obtained for the Loess soil. The capillary pressure ψ is in hPa.

properties are mainly governed by the pore size distribution and topology and that the quantitative approach to describe these properties is promising - at least for the material investigated here.

The significance of topology becomes evident in case the topological characteristics are ignored for the network simulations (Fig. 5). Then, the pressure-saturation relation

exhibits a marked air entry point at a critical capillary pressure which corresponds to the percolation threshold of a random network. Accordingly, the shape of the relative hydraulic conductivity function is changed.

4 Topology of Continuous Fields

At the pore scale it is evident that the topological characteristics of the pore space is essential in terms of flow and transport. But also at a larger scale, where individual pores are no more visible, topology may play a crucial role regarding transport in porous media. At this large scale the binary image of the pore structure disappears and is replaced by fields of continuous variables as porosity or permeability. Obviously, the continuity and connectivity of various conductive regions is significant in terms of flow and transport.

The effect of spatial variability is commonly studied through numerical models that solve the governing equations for fluid flow and transport. Such models require an explicit description of the spatial patterns of hydraulic properties which must be deduced from some kind of observations or measurements.

One important aspect is the distribution function of hydraulic properties, as e.g. the hydraulic permeability, which is often found to be lognormal. Another important measure is the correlation scale of the heterogeneous field which may be quantified by the auto-covariance function. These quantities may be inferred from a set of point measurements even in plane sections and can be used for the generation of continuous correlated random fields [33, 36].

Thereby, however, the topological characteristic of the generated spatial pattern is merely an implicit consequence of the generation process. For an explicit consideration of topology, some quantitative criteria are required that address the connectivity of continuous fields. However, the same problems as encountered at the pore scale are to be solved: the requirement of continuous information on the spatial pattern at a spatial resolution corresponding to the size of the structural units which are relevant. As an example, the connectivity of a narrow tortuous band of high permeability cannot be detected by a set of point measurements but requires a continuous map at a resolution below the width of that band. This kind of structure is crucial for flow and transport and is rather the rule than the exception in natural porous media as fractured rocks, sediments and soil. In isotropic media as sandstone however, such features typically do not exist.

Nowadays, there are techniques available which allow a continuous measurement of the structure at high spatial resolution. For the analysis of porous media at a small scale X-ray tomography has become a very efficient tool [19, 35, 39, 21]. On a larger scale different geophysical methods are available. In the following, a connectivity function for continuous fields is introduced which is based on the same concepts as for binary structures. It is demonstrated for the structure of a soil sample obtained from X-ray tomography.

Figure 6 (left) shows a horizontal section through undisturbed soil obtained by a medical X-ray tomograph. Basically, X-ray tomography measures the local X-ray absorption coefficient μ_x which is related to the density of electrons. Hence, assuming homogeneity of the solid phase, i.e. absorption coefficient $\mu_s = const$, and a homogeneous fluid within the pore space characterized by the constant μ_w , the measured

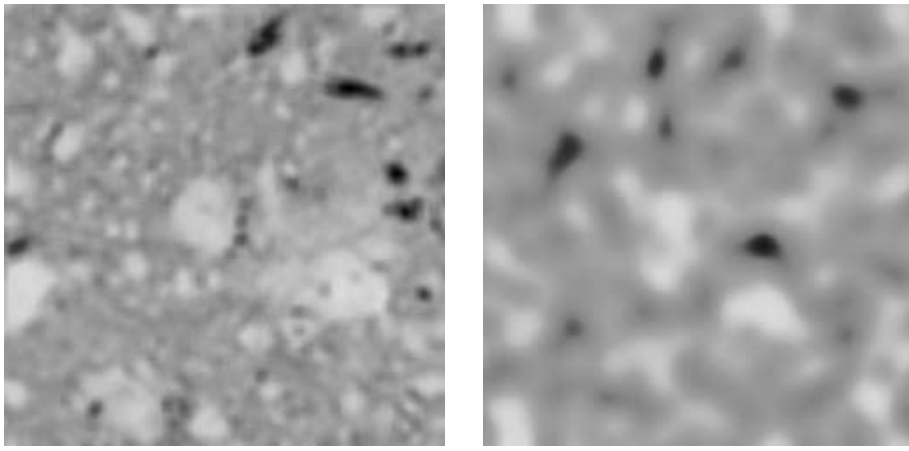

Fig. 6. 2D density image of a Loess soil (left, natural height 110 mm, resolution 0.44 mm) and a Gaussian random field (right) with equivalent grey level distribution and correlation length.

absorption at each location x is given by

$$\mu_x = [1 - \Phi_x]\mu_s + \Phi_x \mu_w \ . \tag{8}$$

Consequently, the porosity Φ_x at each location x can be obtained directly from measurements of μ_x and the image in Fig. 6 may be interpreted as a map of porosity $\Phi(x)$. Moreover, for a given material, the porosity is expected to be closely related to permeability.

The classical approach of modeling this kind of structure is based on the distribution function of Φ expressed by the cumulative density function (cdf) $G(\Phi)$ and the spatial correlation. The latter is quantified by the auto-covariance function $C_\Phi(h)$ which is calculated as

$$C_g(h) = \langle [\Phi(x) - \langle \Phi(x) \rangle][\Phi(x+h) - \langle \Phi(x) \rangle] \rangle \tag{9}$$

where $\langle\rangle$ denotes expectation. The measured structural properties $G(\Phi)$ and $C_\Phi(h)$ are shown in Fig. 7. From (9) the correlation length λ was obtained as

$$\lambda = \frac{1}{\sigma^2} \int_0^\infty C_\Phi(h) \mathrm{d}h \tag{10}$$

where σ^2 is the variance of Φ.

Following the classical approach, a Gaussian random field $f_0(x)$ was generated [1, 33, 36]. Thereby , the same correlation length as measured in the X-ray image was realized. Then, the resulting field $f_0(x)$ was transformed to $f_1(x)$ so that the cumulative density function F of the random field matches the measured distribution $G(\Phi)$:

$$f_1(x) = G^{-1}[F(f_0(x))] \tag{11}$$

As a consequence of such a histogram matching, also referred to as 'nonlinear filtering' [30] the spatial correlation of $f_1(x)$ is changed compared to $f_0(x)$. Thus, the correlation

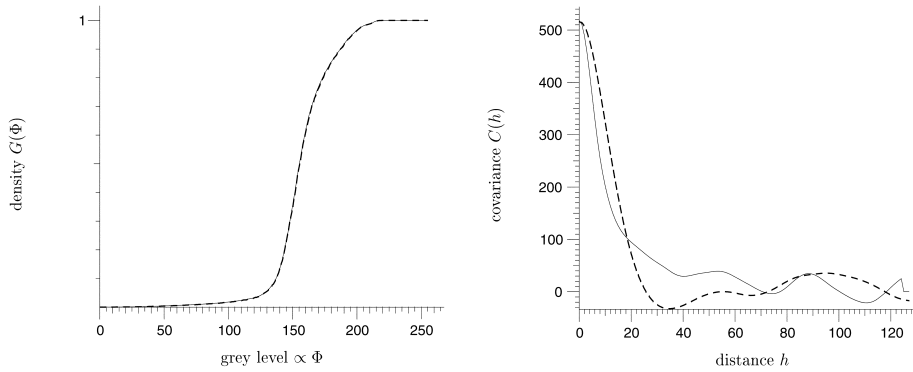

Fig. 7. Density function of porosity $G(\Phi)$ (left) and auto-covariance $C_\Phi(h)$ (right) for the natural structure of soil (thin line) and the correlated random field (dashed line) shown in Fig. 6.

length λ which was used to generate f_x was altered iteratively so that λ of $f_1(x)$ matches that of $g(x)$.

In this way the correlated random field shown in Fig. 6 (right) was generated. As shown in Fig. 7 the distribution function of the random field is identical compared to the original image while the correlation matches only in terms of the correlation length λ. From a qualitative point of view, the modeling approach seems to be appropriate also with respect to connectivity for this two dimensional example.

In order to quantitatively describe the topological characteristics of the continuous fields, the Euler characteristic χ was calculated as a function of a threshold value t. For each t we obtain a binary image (Fig. 9) and a corresponding Euler characteristic which yields the connectivity function $\chi(t)$ for continuous fields. The results for the two-dimensional examples of Fig. 6 are shown in Fig. 8 where the Euler numbers are plotted relative to the maximum value. Clearly, the absolute values of $\chi(t)$ differ considerably because of the smoothness of the random field. However the shapes of the different connectivity functions are rather similar. Starting from low values of t, $\chi(t)$ increases which indicates a number of isolated dark islands, i.e. islands of high porosity (see also Fig. 6). While increasing t further, the structure becomes more and more connected and reaches high negative values which means a considerable number of loops or, from the perspective of the background, a considerable number of isolated islands of low porosity. This behavior is illustrated in Fig. 9 where the extreme values of $\chi(t)$ are represented together with the case for $\chi(150) \approx 0$ which may be related to a percolation threshold [24].

As already mentioned, the random field resembles the original image quite well and one would not expect considerable differences for effective hydraulic conductivity in case the grey values of the two images in Fig. 6 are assumed to represent permeabilities. However, we are looking at a two dimensional cut out from a three dimensional sample and one could easily imagine that the 2D islands of high porosity are intensely connected in three dimensions as could be expected from root holes or earthworm burrows in soil.

In Fig. 10 a three dimensional isosurface ($t = 30$) for the original X-ray image and a 3D Gaussian random field is shown. Again, the correlation lengths and the distribution

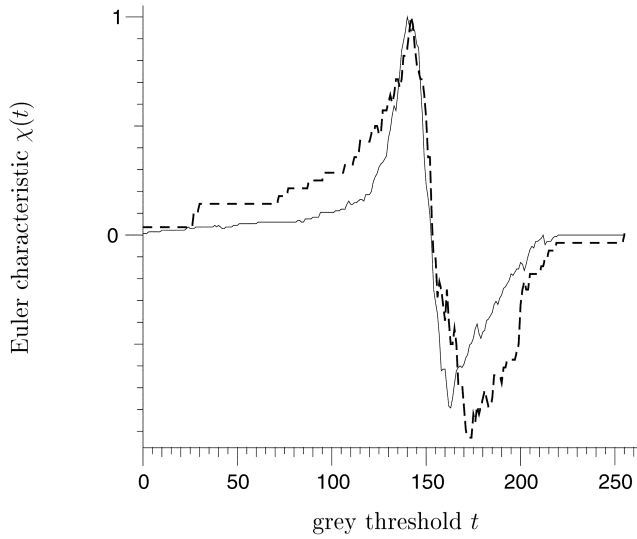

Fig. 8. 2D Connectivity functions of the porosity image (thin line) and the correlated random field (dashed line) shown in Fig. 6. The Euler numbers are plotted relative to the maximum values.

functions are the same for both structures. However the topology in 3D is considerably different. In Gaussian random fields, the extreme values are always located on islands while the highest porosities in the undisturbed soil are related to large pores which typically originate from roots or earthworms and hence, are intensely connected.

In analogy to the two dimensional case discussed above, the 3D connectivity functions $\chi(t)$ was calculated for the two structures which came out to be considerably different as well (Fig. 11). The results clearly confirm the qualitative findings that the random field generates a large number of isolated objects of high porosity $(t < 120)$ while the natural structure is more connected. The same is true for the other extremity of low porosity $(t > 190)$ where the connectivity of low porosity is lower for the random field. In contrast to the two dimensional case, the values for $\chi(t)$ are positive for

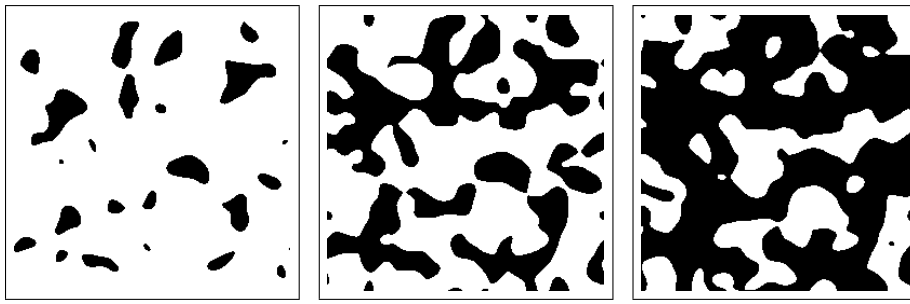

Fig. 9. Gaussian random field of Fig. 6 binarized according to different thresholds $t = 140, 150, 160$ (from left to right)

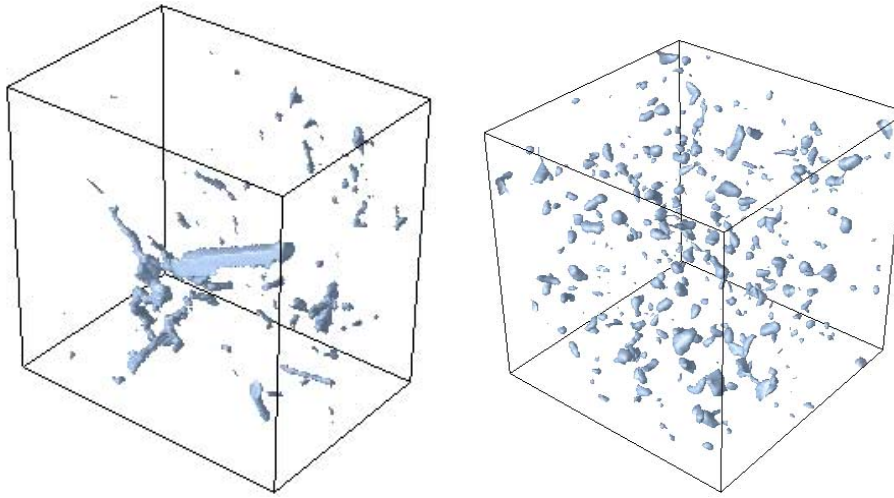

Fig. 10. 3D porosity image of a Loess soil (left, natural height 110 mm, resolution 0.44 mm) and Gaussian random field (right) with equivalent grey level distribution and correlation length. Grey levels below 40 indicating high porosities are marked by isosurfaces.

high values of t because the number of completely enclosed cavities are counted with a positive sign according to (1).

5 Numerical Simulations

To demonstrate the significance of the topological characteristics water flow was simulated in 2-dimensional random permeability fields. The aim was to generate different structures having the same auto-covariance function but different topology.

We start with a Gaussian random field f_0 with correlation length λ_0 and variance σ_0. As already discussed in the previous section, the extreme values of f_0 are located on islands which are not connected. In contrast, the values around the expectation of f_0 are located on connected bands. Thus, the values of f_0 were resorted in a way that the extreme values are located on these connected bands. This was achieved for each location x by

$$f_1(x) = |2f_0(x) - f_{0,\max}| \tag{12}$$

where $f_{0,\max}$ is the maximum value of f_0. Obviously, the histogram of the resulting random field f_1 is affected by this transformation except the values of f_0 are equally distributed in $[f_{0,\mathrm{mim}}, f_{0,\max}]$. For this reason the distribution function of f_0 was tranformed to an equal distribution using (11) prior to the application of (12).

Moreover, also the spatial correlation is affected by (12). In the original random field f_0 the spatial distance between minimum and maximum values is considerably larger as compared to f_1. Consequently, to arrive at two random fields with comparable auto-covariance but different topology, we generated another Gaussian random field f_2 having the same covariance as f_1.

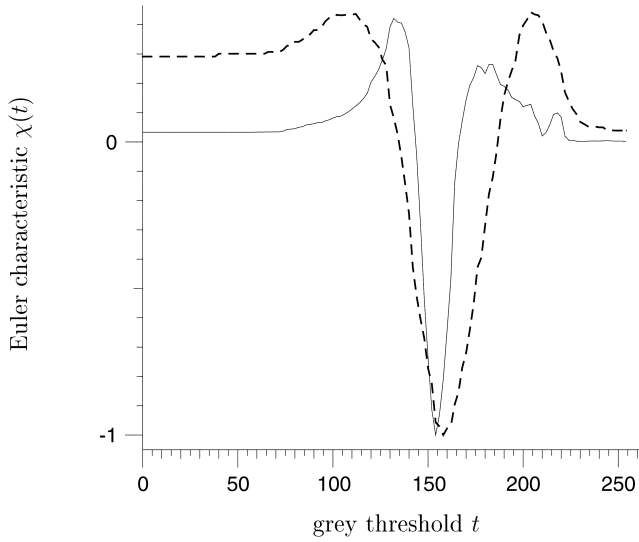

Fig. 11. 3D connectivity function $\chi(t)$ for the 3D X-ray image of soil (line) and the Gaussian random field (dashed line). The Euler characteristics are plotted relative to the maximum value to allow a better comparison of the two curves. The images are shown in Fig. 10

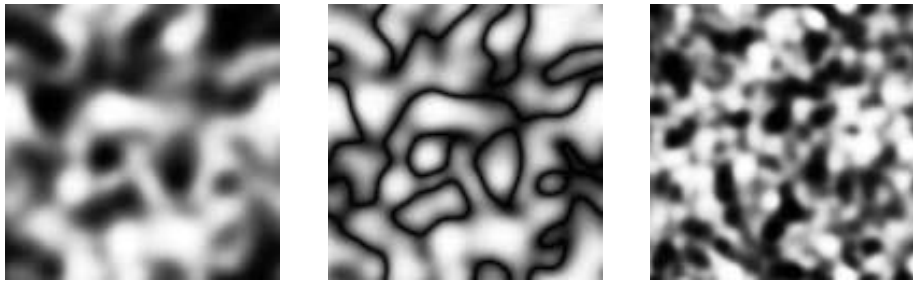

Fig. 12. Gaussian random field f_0 (left) after redistribution according to (12), f_1 (middle) and the Gaussian random field f_2 with the same auto-covariance function as f_1 but different topology.

In Fig. 12 the original random field f_0, the result after redistribution, f_1, and the random field f_2 which was adapted to the auto-covariance of f_1 are shown. The corresponding covariance and connectivity functions are shown in Fig. 13. The topological difference between f_1 and f_2 is clearly reflected by the connectivity function. Increasing the threshold t for the random field f_1 leads to an early drop of the Euler characteristic to slightly negative values indicating the number of loops within the connected dark band through the structure. In contrast, $\chi(t)$ for the Gaussian random fields f_0 and f_2 reflects the isolated clusters of the extreme values.

The next step was to investigate the effect of the topological characteristics on effective properties of the heterogeneous fields. Therefore, the grey values of the random fields were considered to represent the logarithms of the permeability, $\log(K)$. Based

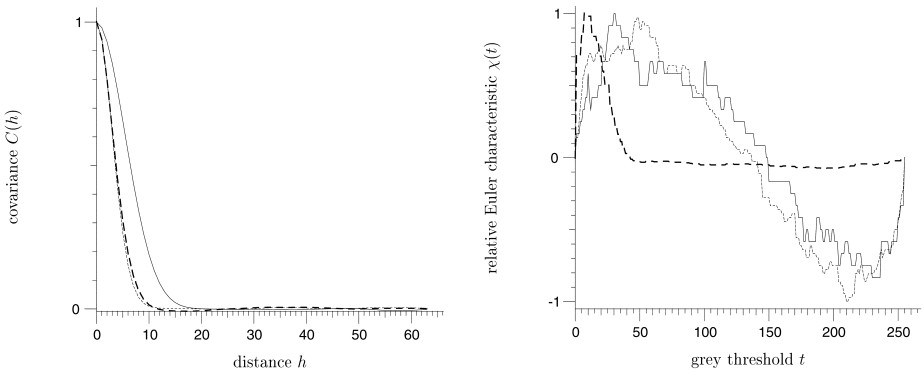

Fig. 13. Covariance and connectivity function for the random fields f_0 (line), f_1 (dashed line), and f_2 (dotted line). The connectivity functions are normalized by the maximum value of $\chi(t)$ for better comparison.

on the resulting structure of permeabilities the velocity field was calculated according to Darcy's law

$$\boldsymbol{u} = K \cdot \nabla p \tag{13}$$

together with the mass balance

$$\nabla \cdot \boldsymbol{u} = 0 \tag{14}$$

which was numerically solved using a finite element scheme. Thereby a pressure gradient from the left to the right edge was simulated with no-flux boundaries at top and bottom.

The resulting velocity fields are presented in Fig. 14. As expected, the velocity field of f_1 is dominated by the continuous band of high permeability. Also for f_2 water flow is concentrated to one single path along which the distances between regions of high permeability are minimal. The effective permeability K_{eff} of f_1 was by a factor of 71.5 higher compared to K_{eff} of f_2. This clearly shows that topology may be critical for effective properties of heterogeneous fields.

6 Conclusions

Topological characteristics of porous media proved to be significant for hydraulic properties and transport both at the pore scale and at a larger scale described by a continuous field of effective material properties. At the pore scale, the proposed connectivity function based on the Euler characteristic together with the pore size distribution allowed a reasonable good prediction of the effective hydraulic properties of a Loess soil.

At the continuum scale, numerical simulations of effective permeabilities for heterogeneous permeability fields evidence the effect of topology also at this scale. Hence, to predict effective properties of porous media in terms of flow and transport, the autocovariance function which is typically used to characterize the spatial heterogeneity is not sufficient. Modeling and quantifying spatial heterogeneity should be supplemented by a topological description. The Euler characteristic as a function of a threshold value

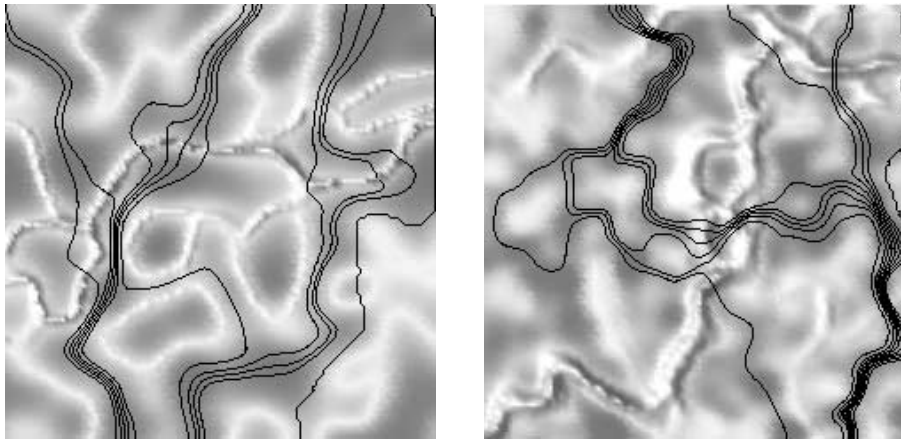

Fig. 14. Field of permeabilities (grey level) and velocity (elevation) together with iso pressure lines for stationary convective flow through the random fields f_1 (left) and f_2 (right). The effective permeability $K_{\rm eff}$ of f_1 is by a factor of 71.5 larger compared to $K_{\rm eff}$ of f_2.

provides a useful connectivity function which quantifies the topological characteristics of continuous fields.

It is a challenge for future research to generate random fields of predefined auto-covariance and predefined topology and to systematically investigate the relation of topology and effective properties.

References

1. P. M. Adler, C. G. Jacquin, J. A. Quiblier, Flow in simulated porous media, Int. J. Multiphase Flow 16 (1990) 691–712
2. C. Arns, M. Knackstedt, K. Mecke, Characterising the morphology of disordered materials, Lecture Notes in Physics (2002), this volume
3. C. Beisbart, R. Dahlke, K. Mecke, H. Wagner, Vector- and tensor-valued descriptors of spatial patterns, Lecture Notes in Physics (2002), this volume
4. B. Berkowitz, I. Balberg, Percolation theory and its application to groundwater hydrology, Water Resources Res. 29 (1993) 775–794
5. M. A. Celia, P. C. Reeves, L. A. Ferrand, Recent advances in pore scale models, Rev.Geophys. 33 (1995) 1049–1057
6. R. Chandler, J. Koplik, K. Lerman, J. F. Willemsen, Capillary displacement and percolation in porous media, J. Fluid Mech. 119 (1982) 249–267
7. I. Chatzis, F. A. L. Dullien, Modeling pore structure by 2-D and 3-D networks with application to sandstone, J. Can. Pet. Technol. 16 (1977) 97–108
8. R. T. DeHoff, Use of the disector to estimate the Euler characteristic of three dimensional microstructures, Acta Stereol. 6 (1987) 133–140
9. I. Fatt, The network model of porous media. I. Capillary pressure characteristics, Pet. Trans. AIME 207 (1956) 144–159
10. I. Fatt, The network model of porous media. II. Dynamic properties of a single size tube network, Pet. Trans. AIME 207 (1956) 160–163

11. I. Fatt, The network model of porous media. III. Dynamic properties of networks with tube radius distribution, Pet. Trans. AIME 207 (1956) 164–181
12. L. A. Ferrand, M. A. Celia, The effect of heterogeneity on the drainage capillary pressure-saturation relation, Water Resour. Res. 28 (3) (1992) 859–870
13. S. Friedman, N. Seaton, On the transport properties of anisotropic networks of capillaries, Water Resour. Res. 32 (1996) 339–347
14. H. Hadwiger, Vorlesung über Inhalt, Oberfläche und Isoperimetrie, Springer-Verlag, Berlin, 1957
15. R. Hilfer, Geometric and dielectric characterization of porous media, Phys. Rev. B 44 (1991) 60
16. R. Hilfer, Local-porosity theory for flow in porous media, Physical Review B 45 (1992) 7115–7121
17. R. Hilfer, Transport and relaxation phenomena in porous media, Adv. Chem. Phys. XCII (1996) 299–424
18. R. Hilfer, T. Rage, B. Virgin, Local percolation probabilities for a natural sandstone, Physica A 241 (1997) 105–110
19. J. W. Hopmans, M. Cislerova, T. Vogel, X-ray tomography of soil properties, In: Tomography of Soil-Water-Root Processes. Eds.: Ande S.H. and J.W. Hopmans. ASA, SSSA Madison, Wisconsin,USA (1994) 17–28
20. G. R. Jerauld, S. J. Salter, The effect of pore-structure on hysteresis in relative permeability and capillary pressure: pore-level modeling, Transort in Porous Media 5 (2) (1990) 103–151
21. M. A. Knackstedt, A. P. Sheppard, M. Sahimi, Pore network modelling of two-phase flow in porous rock: the effect of correlated heterogeneity, Adv. Water Res. 24 (2001) 257–277
22. R. Magerle, Nanotomography, Lecture Notes in Physics (2002), this volume
23. J. Mecke, D. Stoyan, The specific connectivity number of random networks, Adv. Appl. Prob. (SGSA) 33 (2001) 576–583
24. K. Mecke, H. Wagner, Euler characteristic and related measures for random geometric sets, J. Stat. Phys. 64 (1991) 843
25. K. Mecke, Additivity, convexity, and beyond: applications of Minkowski Functionals in statistical physics, Lecture Notes in Physics 554 (2000) 111–184
26. K. Mecke, D. Stoyan, Statistical physics and spatial statistics - the art of analyzing and modeling spatial structures and pattern formation, Lecture Notes in Physics 554.
27. J. Ohser, W. Nagel, K. Schladitz, The Euler number of discretized sets, Lecture Notes in Physics (2002), this volume
28. J. Ohser, W. Nagel, The estimation of the Euler-poincaré characteristic from observations on parallel sections, J. Microsc. 184 (1996) 117–126
29. W. H. Press, S. A. Teukolsky, W. T. Vetterling, B. P. Flannery, Numerical Recipes in C. The Art of Scientific Computing, second edition Edition, Cambridge University Press, Cambridge, 1992
30. J. Quiblier, A new three dimensional modeling technique for studying porous media, J. Colloid Interface Sci. 98 (1984) 84–102
31. H. Rajaram, L. A. Ferrand, M. A. Celia, Prediction of relative permeabilities for unconsolidated soils using pore-scale network models, Water Resour. Res. 33 (1997) 43–52
32. A. P. Roberts, S. Torquato, Chord-distribution functions of three-dimensional random media: approximate first-passage times of gaussian processes, Phys. Rev. E 59 (1999) 4953–4963
33. M. J. L. Robin, A. L. Gutjahr, E. A. Sudicky, J. L. Wilson, Cross-correlated random field generation with the direct fourier transform method, Water Resour. Res. 29 (1993) 2385–2397
34. V. Robins, Computational topology for point data: Betti numbers and α-shapes, Lecture Notes in Physics (2002), this volume

35. H. Rogasik, J. W. Crawford, O. Wendroth, I. M. Young, M. Joschko, K. Ritz, Discrimination of soil phases by dual energy X-ray tomography, Soil Sci. Soc. Am. J. 63 (1999) 741–751
36. K. Roth, Steady state flow in an unsaturated, two-dimensional, macroscopically homogeneous, miller-similar medium, Water Resources Res. 31 (1995) 2127–2140
37. J. Serra, Image Analysis and Mathematical Morphology, Academic Press, London, 1982
38. D. C. Sterio, The unbiased estimation of number and sizes of arbitrary particles using the disector, J. of Microsc. 134 (1984) 127–136
39. V. C. Tidwell, L. C. Meigs, T. Christian-Frear, C. M. Boney, Effects of spatially heterogeneous porosity on matrix diffusion as investigated by X-ray absorption imaging, J. Contam. Hydrol. 42 (2000) 285–302
40. H. J. Vogel, Digital unbiased estimation of the Euler-Poincaré characteristic in different dimensions, Acta Stereol. 16/2 (1997) 97–104
41. H. J. Vogel, Morphological determination of pore connectivity as a function of pore size using serial sections, Europ. J. Soil Sci. 48 (1997) 365–377
42. H. J. Vogel, K. Roth, A new approach for determining effective soil hydraulic functions, Europ. J. Soil Sci. 49 (1998) 547–556
43. H. J. Vogel, A numerical experiment on pore size, pore connectivity, water retention, permeability, and solute transport using network models, Europ. J. Soil Sci. 51 (2000) 99–105
44. H.-J. Vogel, K. Roth, Quantitative morphology and network representation of soil pore structure, Adv. Water Res. 24 (2001) 233–242
45. A. W. Western, G. Blöschl, R. B. Grayson, Toward capturing hydrologcally significant connectivity in spatial patterns, Water Resour. Res. 37 (2001) 83–97
46. J. Widjajakusuma, C. Manwart, B. Biswal, R. Hilfer, Exact and approximate calculations for the conductivity of sandstones, Physica A 270 (1999) 325–331
47. W. R. Wise, A new insight on pore structure and permeability, Water Resour. Res. 28 (1992) 189–198